Crowding by Anionic Nanoparticles Causes DNA Double-Strand Instability and Compaction

ARTICLE *in* THE JOURNAL OF PHYSICAL CHEMISTRY B · JANUARY 2014

Impact Factor: 3.3 · DOI: 10.1021/jp4107712 · Source: PubMed

4 AUTHORS, INCLUDING:

Anatoly A Zinchenko
Nagoya University
68 PUBLICATIONS **838** CITATIONS
SEE PROFILE

Kanta Tsumoto
Mie University
38 PUBLICATIONS **632** CITATIONS
SEE PROFILE

Kenichi Yoshikawa
Doshisha University
631 PUBLICATIONS **11,958** CITATIONS
SEE PROFILE

THE JOURNAL OF PHYSICAL CHEMISTRY B

Article

pubs.acs.org/JPCB

Crowding by Anionic Nanoparticles Causes DNA Double-Strand Instability and Compaction

Anatoly Zinchenko,*[,†] Kanta Tsumoto,[‡] Shizuaki Murata,[†] and Kenichi Yoshikawa[§]

[†]Graduate School of Environmental Studies, Nagoya University, Nagoya, 464-8601, Japan

[‡]Graduate School of Engineering, Mie University, Mie, 514-8507, Japan

[§]Faculty of Life and Medical Sciences, Doshisha University, Kyotanabe, 610-0394, Japan

Supporting Information

ABSTRACT: Up to the present, DNA structural transitions caused by cationic polymers as well as in concentrated solutions of neutral polymers are well documented, while a little is known about DNA interaction with like-charge species. Herein, changes in the structure of DNA induced by anionic nanoparticles of different sizes (20−130 nm) were investigated by combining single-molecule DNA fluorescent microscopy, to monitor the conformational dynamics of long-chain DNA, with spectroscopic methods, to gain insight into changes in the secondary structure of DNA. The results showed that several percent of negatively charged silica nanoparticles induced DNA compaction from a coil to a globule, and this change was accompanied by a decrease in the melting temperature of the DNA double helix. DNA was compacted into toroidal condensates with reduced diameters of about 20−30 nm. Smaller 20 nm nanoparticles triggered a DNA coil−globule transition at lower concentrations, but the exclusion volume for each type of nanoparticle at the point of complete DNA collapse, as estimated by taking into account the depth of the ionic atmosphere, was found to be almost the same.

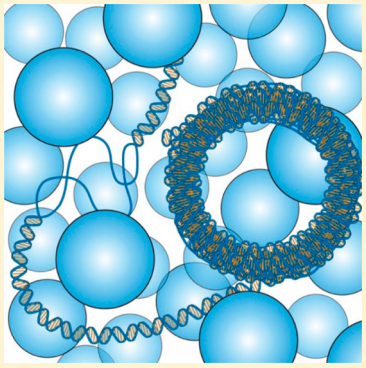

INTRODUCTION

DNA compaction is an important natural mechanism for the storage of extremely long genomic DNAs within the minute space of living cells. In this regard, DNA compaction has been intensively studied both *in vivo* and *in vitro* over the past several decades.[1−4] With the use of *in vitro* model systems, long DNA (above the order of several tens of kilobase pairs (kbp's)) has been shown to condense into compact particles with the addition of multivalent cations,[5,6] cationic polymers,[7−9] cationic nanoparticles,[10] etc., mediated by the electrostatic interaction between negatively charged DNA and cationic binder.[11] Another scenario of DNA compaction is so-called ψ-condensation (polymer and salt-induced = psi) in solutions containing high concentrations of neutral polymers together with high concentrations of monovalent salt.[12−15] This type of condensation is driven by the exclusion volume of neutral polymers due to unfavorable contact between a neutral polymer and DNA in solution. DNA compaction in solutions with large amounts of neutral polymer is considered to be a simple model of DNA condensation in the protein-crowded environment inside living cells.[16,17]

In contrast to the well-established phenomena of DNA condensation by multivalent cations and ψ-condensation, the interaction of DNA, an anionic polyelectrolyte, with like-charge anionic species has attracted very little attention, although many of the most abundant biological polymers, i.e., actin, tubulin, RNA, etc., are negatively charged. Our recent study which sought to compare the changes in the secondary structure of DNA in the presence of 15 nm anionic and cationic nanoparticles at concentrations below 0.1% showed that anionic nanoparticles had essentially no influence on the stability of the secondary structure of DNA.[18] Very recently, however, Vasilevskaya et al.[19] and Yoshikawa et al.[20] reported that, in the presence of about 15% highly negatively charged albumin protein, DNA undergoes a coil−globule conformational transition at the level of single DNA molecules, and this transition was discussed in terms of depletion interactions. Importantly, the salt effect in DNA compaction by negatively charged protein was found to be different from classical ψ-condensation—DNA compaction in a concentrated albumin solution was inhibited by an increase in the salt concentration.[20]

Inspired by these recent findings regarding DNA compaction in like-charge protein solutions, we studied changes in the conformation of DNA in a simpler artificial system containing only long DNA and high concentrations of anionic silica (SiO_2) nanoparticles (20−130 nm), at the level of single DNA molecules. In comparison with the protein-induced DNA compaction reported earlier, silica nanoparticles can be considered to be nonspecifically interacting nanospheres, and their effect on DNA might be explained in terms of a simpler consideration of electrostatics and the exclusion volume. Since silica nanoparticles can vary in size, it may be possible to gain a deeper understanding of the mechanism that underlies changes

Received: November 1, 2013
Revised: January 14, 2014
Published: January 14, 2014

dx.doi.org/10.1021/jp4107712 | J. Phys. Chem. B 2014, 118, 1256−1262

in the structure of DNA induced by polyanionic species. In the present study, we also used spectroscopic methods to study the changes in the secondary structure of DNA (stability of the double helix) to clarify the correlation between the secondary and higher-order structures of DNA induced by negatively charged silica nanoparticles.

MATERIALS AND METHODS

Materials. T4 DNA was purchased from Nippon Gene Co. Ltd. (Japan), and salmon sperm DNA was purchased from Wako Pure Chemical Industries Ltd. (Japan). Throughout the manuscript, the concentration of DNA is given as the concentration of DNA phosphate groups (i.e., monomer units). Silica nanoparticles, organosilicasols IPA-ST-MS, IPA-ST-L, and IPA-ST-ZL, abbreviated herein as M, L, and X, respectively, were a gift from Nissan Chemical Industries Ltd. (Tokyo, Japan). The nanoparticles contain 15−16% amorphous SiO_2, 84−85% H_2O, and less than 0.03% Na_2O according to the manufacturer. The fluorescent dye YOYO-1 (1,1′-(4,4,7,7-tetramethyl-4,7-diazaundeca-methylene)-bis-4-[3-methyl-2,3-dihydro-(benzo-1,3-oxazole)-2-methylidene]-quinolinium tetraiodide) was provided by Molecular Probes (Invitrogen, Japan). Quant-iT PicoGreen dsDNA Reagent for determining the proportion of double-stranded DNA was purchased from Invitrogen (Japan). NaCl and spermine tetrahydrochloride were purchased from Nacalai Tesque Inc. (Kyoto, Japan). Deionized water (Milli-Q, Millipore) was used in all experiments.

Silica Nanoparticles Stock Solutions. Approximately 30% 2-propanol dispersions of nanoparticles provided by the manufacturer were dried at 120 °C for 3 h on a hot plate to remove solvent until the mass remained constant. The resulting powder was suspended in twice the weight of Milli-Q water by ultrasonic sonication at 20 kHz for 30 min to give a 33.3% stable suspension that was used for the experiments. The percentage concentrations of nanoparticles are given as w/w concentrations, which are roughly equivalent to v/v concentrations used for calculations because the specific gravity of nanoparticles (NPs), as reported by the manufacturer, is 0.96−1.02. Solutions of nanoparticles show acidic pH's, as shown in Table 1, e.g., 1.00% M, L, and XL nanoparticles in the presence of 1 mM NaCl have pH 3.9, 4.0, and 5.8, respectively.

Table 1. Average Diameter, Zeta Potential, and pH of M, L, and X Nanoparticles

nanoparticle	diameter measured by TEM (nm)	zeta potential[a] (mV)	pH of 1% NP solution[a]
X	135 ± 8	−30 ± 15	5.8
L	55 ± 10	−35 ± 15	4.0
M	21 ± 4	−25 ± 6	3.9

[a]The pH of 1 mM NaCl solution without NPs was 6.3.

UV−vis Spectroscopy of the DNA Melting Transition. UV spectra of salmon sperm DNA were recorded on a Jasco U-550 UV/vis spectrophotometer equipped with an ETC-505T thermo-controller (Jasco, Japan) in 1.0 cm × 1.0 cm × 0.5 cm quartz cells, the contents of which were constantly stirred by a magnetic stirring bar during measurements. UV absorbance at 260 nm was recorded against reference solutions that contained the same concentration of NPs as in the sample solution with DNA. After DNA and NPs were mixed, the sample was incubated in a spectroscopic cell for 30 min under magnetic stirring before measurement. The temperature gradient in DNA denaturation experiments was set to 1 °C/min. The reproducibility of DNA denaturation curves was examined by repeating the melting experiment three times, and the results confirmed that the fluctuation of T_m did not exceed 1 °C.

Fluorescent Spectroscopy Measurements of the DNA Double Helix Ratio. Fluorescence spectra of PicoGreen (200-fold diluted stock solution provided by the manufacturer) in solutions containing 1 μM (in phosphates) salmon sperm DNA were recorded on a FP-6600 spectrofluorometer in 1.0 × 1.0 × 5.0 cm^3 quartz cells at room temperature following the protocol provided by Invitrogen (Japan). The protocol is available at http://tools.lifetechnologies.com/content/sfs/manuals/mp07581.pdf. In brief, to 1 mL of a solution of salmon sperm DNA that was mixed with an appropriate concentration of nanoparticles (which are twice as large as those in Figure 4A) and incubated for 10 min was added 1 mL of a PicoGreen solution with gentle mixing. After 5−10 min of incubation, PicoGreen fluorescence spectra were recorded. The control experiment with spermine was performed in exactly the same manner.

Fluorescence Microscopy (FM). Sample solutions were prepared by successive mixing of water, NaCl solution (1 mM), nanoparticles, the fluorescent dye YOYO (20 nM), and T4 DNA (100 nM). After the solution components were gently mixed, the resulting samples were incubated for 30 min prior to observations. FM observations were performed using an Eclipse TE2000-U (Nikon, Japan) microscope equipped with an oil-immersion lens. Fluorescent images were recorded and analyzed using an EB-CCD camera and an Argus 10 image processor (Hamamatsu Photonics, Japan).

Transmission Electronic Microscopy (TEM). TEM observations were performed at room temperature using a HITACHI H-800 microscope (Japan) at an acceleration voltage of 200 kV. For TEM observations of nanoparticles, a 3 mm copper grid covered with a collodion film was placed on a drop of the solution containing ca. 0.5% nanoparticles. After 5 min, blotted solution was removed with filter paper, and the sample was dried at room temperature before observation. For TEM observations of compacted DNA, 300 μL of 10 μM T4 DNA in 1 mM NaCl solution was mixed with an appropriate amount of 33.3% solution of M nanoparticles. The samples were incubated for 15 min, and a drop of the sample was placed on a 3 mm copper grid covered with a collodion film and incubated for 5 min. After 5 min, blotted solution was removed with filter paper, after which the grid was placed on a drop of 2% uranyl acetate water solution for DNA staining and incubated for 3 min. Finally, the drop of uranyl acetate was wiped with filter paper and the sample was dried at room temperature before observations.

Zeta-Potential Analysis. The zeta potentials of nanoparticles were measured by a Zetasizer Nano ZS (Malvern, England) in 1 mM NaCl aqueous solution at room temperature.

Sodium Ion Selective Electrode. The concentration of sodium ions in aqueous solution was measured by an F-23 model pH/ion meter (Horiba, Japan) equipped with Na^+ selective electrode 1512A (Horiba, Japan) at room temperature.

RESULTS

Single-Molecule Observation of DNA Conformational Dynamics in Solutions of Silica Nanoparticles. Silica

dx.doi.org/10.1021/jp4107712 | J. Phys. Chem. B 2014, 118, 1256−1262

nanoparticles were characterized by transmission electron microscopy (TEM) and zeta potential measurements. TEM images of X, L, and M silica nanoparticles (NPs) are shown in Figure 1 together with the corresponding size distributions measured over at least 100 NPs. The average size of each type of NP is summarized in Table 1 and is equal to 20 nm for M, 55 nm for L, and 130 nm for X. Table 1 also shows the results of zeta-potential measurements, according to which each type of NP in 1 mM NaCl solution is a highly negatively charged species (zeta potential ca. −30 mV).

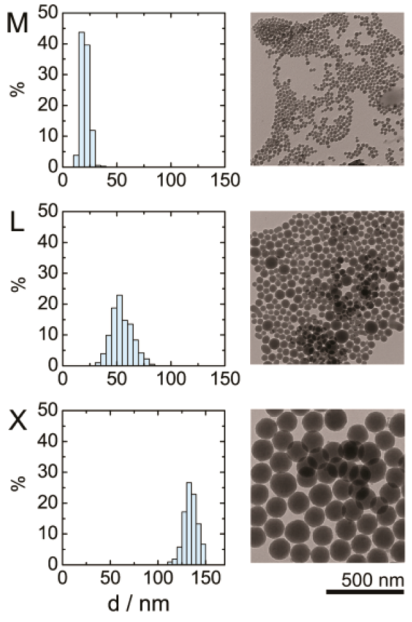

Figure 1. Transmission electron microscopy images (right) and diameter distributions of M, L, and X silica nanoparticles (left) analyzed statistically by measuring at least 100 particles in each sample.

Due to the complex character of the investigated systems, all the experiments were performed in solutions containing only 1 mM NaCl. Although such NaCl concentration is significantly lower than physiological salt, it was chosen to eliminate the aggregation effect of NPs which inevitably occurred at higher ionic strengths.

Silica nanoparticles were mixed with 1 mM NaCl solutions of YOYO-labeled T4 DNA (ca. 166 kbp), and DNA molecules that exhibited Brownian motion were observed by fluorescence microscopy (FM). The results of single-molecule observations of the conformational dynamics of giant DNA at various concentrations of X, L, and M NPs are shown in Figure 2A. The addition of nanoparticles of any size to DNA solutions induced a change in the conformation of DNA from an elongated coil (Figure 2A, 0%, FM image inset) with an average long-axis length of ca. 5 μm to a compact globule of smaller than 1 μm (Figure 2A, L NP 8.64%, FM image inset). It should be noted that, in fluorescence microscopy, an object that is smaller than 1 μm appears as an optical dot due to the blurring effect.[21] Corresponding distributions of DNA long-axis lengths measured from fluorescence profiles are shown in Figure 2A, and indicate that the compaction of DNA by anionic NPs occurred at concentrations that ranged from 2% (for small M NPs) to about 10% (for large X NPs). With X and L

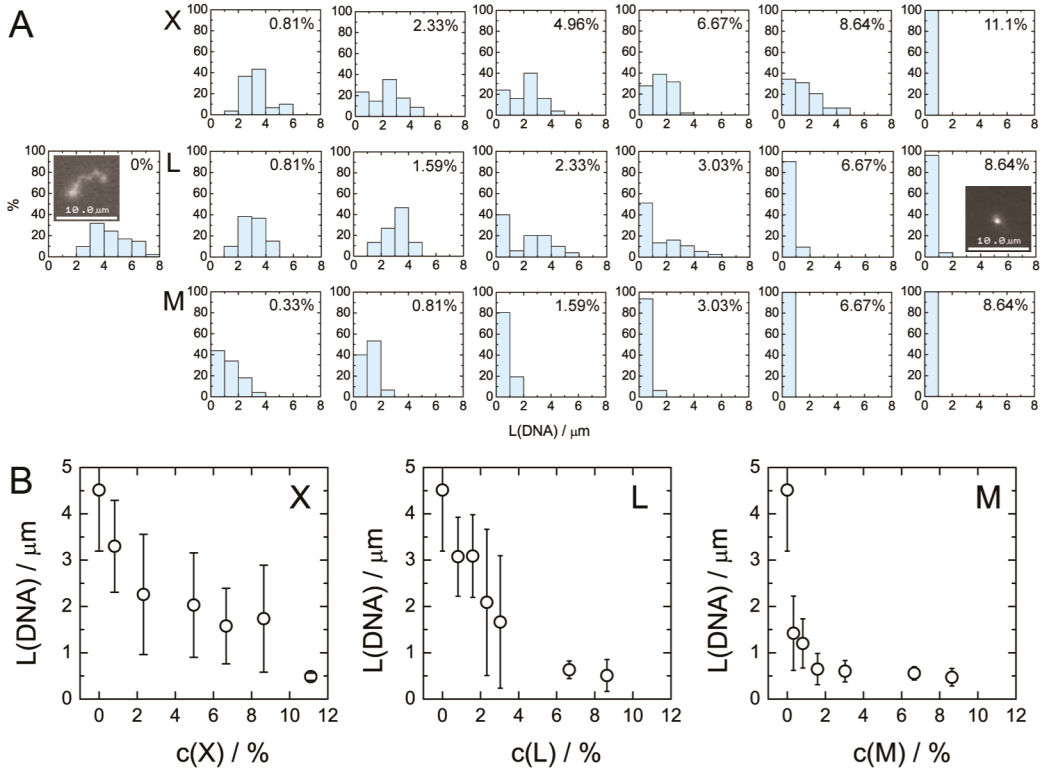

Figure 2. Single-molecule observations of DNA compaction by silica nanoparticles. (A) Long-axis length distributions of individual T4 DNA molecules in 1 mM NaCl solutions of X, L, and M nanoparticles at different concentrations. Insets: typical fluorescence microscopy images of YOYO-labeled T4 DNA molecules in the coil (0% histogram) and globule (8.64% L) states. The scale bars are 10 μm. (B) Changes in the average long-axis length of T4 DNA molecules as a function of the concentrations of X (left), L (middle), and M (right) nanoparticles in 1 mM NaCl solutions. The error bars indicate the standard deviations of the average values measured over at least 50 individual DNA chains.

dx.doi.org/10.1021/jp4107712 | J. Phys. Chem. B 2014, 118, 1256−1262

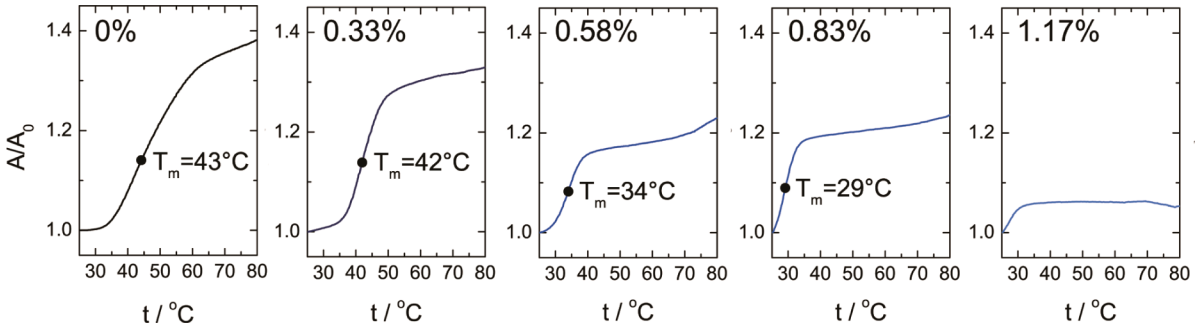

Figure 3. DNA denaturation (melting) curves in solutions of M nanoparticles at different concentrations. Temperature dependence of normalized salmon sperm DNA (100 μM) absorbance (A/A_0) at 260 nm in 0, 0.33, 0.58, 0.83, and 1.17% solutions of M nanoparticles, respectively, recorded against DNA-free reference solutions containing the same concentrations of M nanoparticles under a temperature gradient of 1 °C/min. The values of T_m (melting temperature) were calculated as the temperatures at the maximum values in the differentiation curves (i.e., at the inversion points in the melting S-curve).

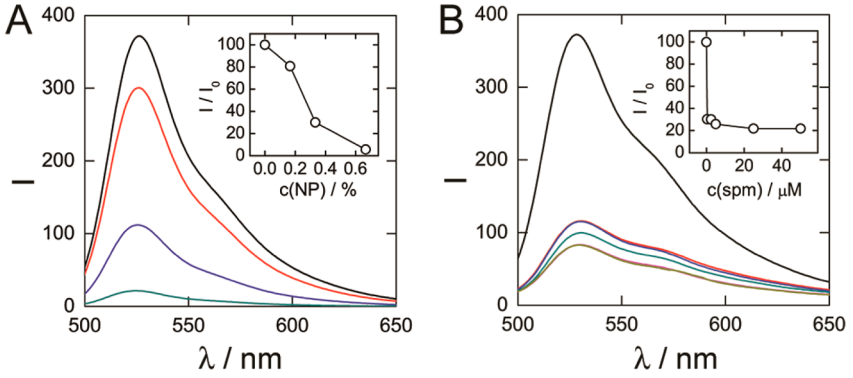

Figure 4. (A) Fluorescence spectra of the fluorescent dye PicoGreen in 1 mM NaCl solution of 1 μM salmon sperm DNA containing increasing concentrations of M nanoparticles (0, 0.17, 0.33, and 0.67% from top to bottom, respectively). The inset shows the dependence of the normalized fluorescence intensity of PicoGreen (I/I_0) at λ = 526 nm on the concentration of M nanoparticles. (B) The control experiment in which different amounts of spermine (0, 0.5, 2.5, 5, 25, and 50 μM from top to bottom, respectively) were added to a solution of salmon sperm DNA under the same conditions as in part A. The inset shows the dependence of the normalized fluorescence intensity of PicoGreen (I/I_0) at λ = 526 nm on the concentration of spermine.

nanoparticles, DNA compaction proceeds as a gradual decrease of the average size of the long-axis length of DNA coil long-axis length. However, one can notice the appearance of an all-or-none-like conformational change on the level of individual DNA molecules; i.e. at the intermediate stages of DNA compaction (e.g., 2.33 and 4.96% X NPs or 2.33 and 3.03% L NPs), a coiled state of about 4.5 μm coexists with a globule state smaller than 1 μm. In contrast, M nanoparticles induce the drastic shrinking of DNA even at a very low concentration; therefore, the type of transition (either continuous or discontinuous) cannot be reliably assigned.

Figure 2B summarizes the data in Figure 2A and shows DNA compaction curves for each type of nanoparticle in terms of the dependence of the average long-axis length of DNA on the NP weight concentration in solutions. Each type of NP induced DNA compaction into globules similarly to L NPs in Figure 2A, but the NP size clearly influenced the concentration at which DNA compaction occurred: the largest X nanoparticles induced DNA compaction at ca. 10%, while small M nanoparticles were very efficient for DNA compaction, and only compact T4 DNAs were observed at concentrations of M NPs higher than 2%. The nature of the decrease in the DNA long-axis length was also different between larger and smaller nanoparticles. For example, 130 nm NPs induced gradual shrinking of DNA and abrupt DNA compaction into globules within a narrow concentration region between 9 and 11%. On the other hand, 20 nm NPs produced dramatic DNA coil shrinking; the addition of only 0.1% M nanoparticles caused the DNA long-axis length to decrease from 4.5 to 1.5 μm, which corresponds to a 30-fold change in the molecular volume of the DNA coil, and DNA was compacted into globules under a doubling of the concentration of NPs.

Changes in the Secondary Structure of DNA Induced by Anionic Nanoparticles. To gain insight into changes in the secondary structure of DNA that accompanied the transition in the higher-order structure of DNA described above, we next studied the stability of the secondary structure of DNA by UV−vis spectroscopy of DNA thermal denaturation (melting). Typically, DNA undergoes a transition from double-stranded DNA to single-stranded DNA upon heating, which can be detected as an approximately 1.4-fold increase in DNA absorbance at 260 nm, as shown in Figure 3 (0%). For spectroscopic experiments that require higher DNA concentrations, we used DNA from salmon sperm. Due to instrumental limitations regarding the observation of turbid samples, i.e., solutions containing L and X nanoparticles, only the influence of small M NPs was investigated. Absorbance at 260 nm in samples containing 100 μM DNA and nanoparticles at concentrations from 0 to 1.17% in 1 mM NaCl was recorded against reference solutions that contained the same concentrations of nanoparticles upon heating from 25 to 80 °C at a temperature gradient of 1 °C/min. Due to the relatively low

dx.doi.org/10.1021/jp4107712 | J. Phys. Chem. B 2014, 118, 1256−1262

ionic strength in 1 mM NaCl solution, the DNA melting in the original NP-free solution occurs between 40 and 70 °C (the melting point T_m is 43 °C) in agreement with earlier reports on the NaCl effect in DNA denaturation.[22] Figure 3 shows that the addition of M nanoparticles from 0 to 1.17% induced two dramatic changes in the melting curves: (1) the DNA melting temperature (the inversion point in the melting S-curve) shifted to lower temperatures, from T_m = 43 °C to below 30 °C, and (2) the overall change in absorbance decreased from 1.4- to 1.05-fold. These changes are ascribed to (1) a decrease in the amount of available DNA for melting with the addition of nanoparticles due to DNA gradual compaction in agreement with the results of fluorescence microscopy and (2) a decrease in the stability of the remaining fraction of noncompacted DNA fraction. For example, at 1.17% M nanoparticles, there was only a very slight increase in the optical density of DNA at the beginning of DNA melting at 25−30 °C, while there were essentially no changes in absorbance after a further increase in temperature. This small increase in DNA absorbance corresponds to less than 15% of the available for denaturation DNA in the sample, and this denaturation occurs at very low temperatures. The results of FM observations combined with DNA melting curves obtained by spectroscopy analysis suggest the mechanism of DNA compaction, according to which addition of nanoparticles to DNA induces simultaneous DNA compaction and destabilization of the remaining noncompacted DNA.

However, the above data give no information on the state of the DNA helix in the compact condensate. Therefore, to provide further insight by another independent method, we used a fluorescence assay based on PicoGreen, a double-stranded DNA dye, the fluorescence of which dramatically increases in the presence of double-stranded DNA but not single-stranded DNA. Figure 4A shows the fluorescence spectra of PicoGreen in 1 μM salmon sperm DNA solution containing from 0 to 0.67% M nanoparticles. Figure 4A shows that the addition of M nanoparticles to DNA solution causes a drastic decrease in the fluorescence intensity of PicoGreen. However, DNA compaction itself can cause a partial release of fluorescent dye from DNA, which is a typical behavior for most DNA intercalators or groove binders. To elucidate the role of DNA compaction in the decrease in fluorescence intensity, we performed a control experiment by adding a typical DNA-condensing tetracation, spermine, to DNA to induce DNA compaction (Figure 4B), and measured the fluorescence of PicoGreen. During DNA compaction by spermine at a concentration of 1 μM, the fluorescence of PicoGreen decreased to about 20% of the original value, and there were no changes at higher concentrations of spermine. The compaction of salmon sperm DNA by spermine at concentrations of 1 μM and higher was confirmed by FM observation of the same samples used for fluorescent spectroscopy analysis. However, in DNA solution that contained high concentrations of nanoparticles, the decrease in fluorescence was significantly greater, i.e., down to 5% of the initial fluorescence (Figure 4).

Similarly, PicoGreen-labeled T4 DNA was observed by fluorescence microscopy at different concentrations of M nanoparticles to directly monitor the changes in fluorescence of PicoGreen at the level of single DNA molecules (Figure 5). The decrease in the DNA long-axis length at high NP concentrations correlated well with the observations of YOYO-labeled DNA (Figure 2). However, when the concentration of M NPs increased (1.39% M), the fluorescent

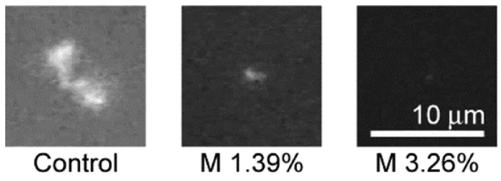

Figure 5. Typical fluorescent images of PicoGreen-labeled single T4 DNA molecules observed in 1 mM NaCl solution containing 0, 1.39, and 3.26% M nanoparticles.

images of strongly shrunken DNA became pale, and at the point of complete DNA collapse (3.26% M), it was difficult to distinguish fluorescent images of DNA globules due to their very low intensity. Since we did not observe the fluorescence quenching of compact YOYO-labeled DNA (Figure 2, FM insets), the quenching of fluorescent images of PicoGreen-labeled DNA during compaction (Figure 5) provided strong evidence of the ineffective fluorescent staining of compacted DNA by PicoGreen. Therefore, in combination with the results regarding the thermal denaturation of DNA, the PicoGreen assay supports our suggestion regarding the partial denaturation of DNA in concentrated solutions of anionic nanoparticles.

The promotion of the DNA helix−coil transition by negatively charged NPs may be related to a change in activity of Na^+ counterions that generally stabilize the DNA double-helical structure diminishing repulsion between DNA helixes. Na^+ selective electrode measurements in solutions with an increasing amount of M nanoparticles indicate that the activity of Na^+ changes from 1 mM in solution without nanoparticles to 2.2 and 2.5 mM in solutions containing 0.83 and 1.67% M nanoparticles, respectively, and thus is not considered to play a role in destabilization of the DNA helix. A change in solution pH caused by the addition of nanoparticles of acidic nature (Table 1) can be another factor to promote DNA denaturation. However, addition of 1% M nanoparticles to DNA solution caused only a little change in pH, i.e., from 7.1 (DNA in 1 mM NaCl solution) to 6.8 (DNA and 1% NPs in 1 mM NaCl solution), which is within the pH range where no DNA structural changes occur.[23] Therefore, it is concluded that destabilization of DNA is caused by crowding with anionic species rather than by changes in concentration of low-molecular-weight electrolytes in DNA solution.

Morphology of Compact DNA Condensates. Transmission electron microscopy (TEM) was used to observe the morphology of DNA in the globular state in concentrated solutions of anionic nanoparticles. Figure 6A shows a TEM image of T4 DNA (10 μM) in a 3.0% solution of M

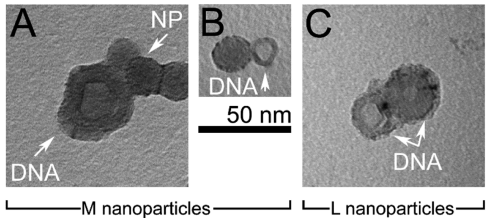

Figure 6. Transmission electron microscopy images of T4 DNA (A) or salmon sperm DNA (B) compacted by M nanoparticles and T4 DNA compacted by solutions of L nanoparticles (C). The concentration of either nanoparticle was 3.0%. The samples were stained with 2% uranyl acetate to increase the contrast of compacted DNAs. The spherical objects in parts A and B are M nanoparticles.

dx.doi.org/10.1021/jp4107712 | J. Phys. Chem. B 2014, 118, 1256−1262

nanoparticles stained with uranyl acetate; we see a toroidal structure with an inner diameter of about 15 nm and an outer diameter of 40 nm. Due to a high concentration of NPs in the TEM sample, the condensates of DNA were frequently found attached to NPs. A similar structure of DNA condensate was observed when T4 DNA was compacted with larger L nanoparticles: condensates consisted of two toroids with a very small inner diameter of about 10 nm (Figure 6C). When short salmon sperm DNA was used, the toroidal morphology and the inner diameter of DNA condensates was intact, while the thickness was only several nanometers (Figure 6B).

According to the available literature, the compaction of DNA by cationic binders such as spermine or in solutions of neutral polymers often leads to the folding of DNA into compact particles with a toroidal morphology.[24,25] In previous reports, typical DNA toroidal condensates were reported to measure around 50−100 nm, as determined mainly by the rigidity of the DNA double helix; i.e., its persistence length exhibits a similar size.[26] Therefore, DNA toroids formed as a result of DNA collapse in solutions of anionic NPs are significantly smaller than the typical DNA toroid dimensions reported so far. This difference can be ascribed to the partial denaturation of the secondary structure of DNA as revealed by spectroscopic analysis. The rigidity of single-stranded DNA is known to be significantly lower than that of double-stranded DNA.[27] Therefore, disturbance of the double-helical structure causes a drastic decrease in the persistence length and thus may promote the formation of a smaller nucleation center (loop), around which the remaining DNA wraps to complete compaction.

DISCUSSION

An earlier report[19] suggested the universality of the phenomenon of DNA compaction in a solution of negatively charged species, and here we provide the first supporting evidence using anionic silica nanoparticles, which, like anionic globular protein, induce DNA collapse at concentrations of just a few percent, whereas in actual living cells the weight percent of macromolecules is on the order of 5−40%. The results of our single-molecule observations of the conformational behavior of DNA made it clear that, in concentrated solutions of negatively charged nanoparticles, DNA undergoes compaction into condensates with a toroidal morphology. Since the efficiency of DNA compaction strongly depends on the size of nanoparticles, we can consider the mechanism of DNA compaction based on the depletion of the DNA coil due to the excluded volume of nanoparticles. If we define the radius of the nanoparticles as R and the Debye length as λ, then the effective volume of the particles should be given as $V = (4/3)\pi(R + \lambda)^3$. If we roughly consider λ to be ca. 10 nm in 1 mM NaCl, the ratio between the total excluded volume and the actual particle volume given as $(R + \lambda)^3/R^3$ should strongly increase with a decrease in the nanoparticle radius from ca. 67 to 10 nm. On the basis of the concentration of NPs when DNA compaction was observed by FM and the ratio $(R + \lambda)^3/R^3$, Figure 7 shows the calculated excluded volumes of X, L, and M nanoparticles that are necessary for complete DNA compaction into globules ($V = c \times ((R + \lambda)^3/R^3)$), where c is the lowest concentration of NPs at which 100% of the analyzed DNA molecules were compacted (Figure 2). The concentrations of NPs in Figure 2 are expressed as w/w, but for the calculations, we treated the same concentrations as v/v, which is appropriate because the specific gravity of nanoparticles is within the range

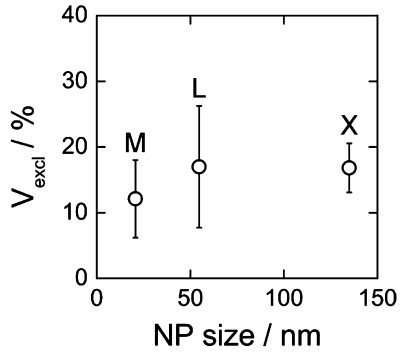

Figure 7. Dependence of the calculated NP excluded volume at which T4 DNA was compacted on the NP diameter. The excluded volume of NPs was calculated from the nanoparticle concentration at which DNA was completely folded into globules. The error bar shows the difference between the excluded volumes calculated from the minimum NP concentration in Figure 2 when DNA was completely compacted (experimental points in the graph) and the maximum NP concentration at which noncompact DNA conformations were still observed.

0.96−1.02. Although the DNA compaction concentrations depend on the size of nanoparticles, the calculated values of the excluded volumes of NPs at the point of DNA collapse are similar, at around 15−20%; i.e., the compaction of DNA takes place at a comparable degree of NP crowding. It is important to note that these values of excluded volume are probably underestimated due to (i) contribution from the DNA excluded volume and (ii) the Debye lengths may be larger than the values we used to estimate the exclusion volumes.[28] Therefore, we speculate that the observed critical concentrations of nanoparticles approach the overlapping concentration, which is ca. 74% for most densely packed spheres. In regard to the charge on NPs, it is to be noted that the anionic charge on NPs is critical for the enlargement of excluded volume, as the excluded volume of neutral hard spheres is roughly determined by their actual geometrical size. In addition, low ionic strengths chosen in the present study play an important role to decrease the NP concentration necessary for DNA compaction to several percent due to increase of the Debye lengths. In contrast, in the earlier report, DNA compaction by negatively charged proteins was performed at high ionic strength (150 mM NaCl) where more than 20% of crowding agent in solution was required to induce DNA collapse.[20]

Besides the excluded volume mechanism, the effect of electrostatics can be manifested in two opposite ways. On one hand, the presence of several percent concentration of hard NP spheres decreases the available for cations solvent volume and this results in the increase of the effective concentrations (activities) of monovalent salt. On the other hand, the addition of anionic nanoparticles may lead to the decrease of cation Na^+ concentration due to their electrostatic interaction with a large anionic surface of nanoparticles. Na^+ selective electrode measurements in solutions with an increasing amount of nanoparticles indicate that the activity of Na^+ changes from 1 mM in solution without nanoparticles to 1.0, 1.5, and 2.3 mM in solutions containing 1.0% X, L, and M nanoparticles, respectively. This change corresponds to the effective change of the excluded volume of NPs. Nevertheless, the change of the activity of Na^+ is minor from the viewpoint of necessary ionic strength for DNA condensation and, thus, can be neglected, providing additional evidence that the DNA phase transition

dx.doi.org/10.1021/jp4107712 | J. Phys. Chem. B 2014, 118, 1256−1262

occurs predominately as a result of the excluded volume effect of anionic nanoparticles as discussed earlier.[19]

Finally, it should be stressed that the compaction of DNA in the present systems was studied in low salt solution (1 mM NaCl) to avoid NP aggregation; therefore, it should be further developed toward understanding the influence of anionic NP crowding under biologically relevant conditions.

■ ASSOCIATED CONTENT

Supporting Information

Original melting curves of DNA in solutions of nanoparticles and control fluorescence spectra of PicoGreen in 1 mM NaCl solution and in the presence of M nanoparticles. This material is available free of charge via the Internet at http://pubs.acs.org.

■ AUTHOR INFORMATION

Corresponding Author

*E-mail: zinchenko@urban.env.nagoya-u.ac.jp. Phone: +81-052-789-4707.

Notes

The authors declare no competing financial interest.

■ ACKNOWLEDGMENTS

This work was supported in part by JSPS and REBR under the Japan-Russia Research Cooperative Program. K.Y. acknowledges the support by Kakenhi (23240044, 25103012). We gratefully acknowledge the High Voltage Electron Microscope Facilities at EcoTopia Science Institute, Nagoya University, and especially Dr. S. Arai for assistance with the TEM observations. We also thank Prof. V.V. Vasilevskaya (Russian Academy of Science) for fruitful discussions.

■ REFERENCES

(1) Teif, V. B.; Bohinc, K. Condensed DNA: Condensing the Concepts. *Prog. Biophys. Mol. Biol.* **2011**, *105* (3), 208−222.
(2) Bloomfield, V. A. DNA Condensation. *Curr. Opin. Struct. Biol.* **1996**, *6* (3), 334−341.
(3) Siber, A.; Dragar, M.; Parsegian, V. A.; Podgornik, R. Packing Nanomechanics of Viral Genomes. *Eur. Phys. J. E: Soft Matter Biol. Phys.* **2008**, *26* (3), 317−325.
(4) Grosberg, A. Y. How Two Meters of DNA Fit into a Cell Nucleus: Polymer Models with Topological Constraints and Experimental Data. *Polym. Sci., Ser. C* **2012**, *54* (1), 1−10.
(5) Yoshikawa, K.; Takahashi, M.; Vasilevskaya, V. V.; Khokhlov, A. R. Large Discrete Transition in a Single DNA Molecule Appears Continuous in the Ensemble. *Phys. Rev. Lett.* **1996**, *76* (16), 3029−3031.
(6) Baumann, C. G.; Smith, S. B.; Bloomfield, V. A.; Bustamante, C. Ionic Effects on the Elasticity of Single DNA Molecules. *Proc. Natl. Acad. Sci. U.S.A.* **1997**, *94* (12), 6185−6190.
(7) Akitaya, T.; Seno, A.; Nakai, T.; Hazemoto, N.; Murata, S.; Yoshikawa, K. Weak Interaction Induces an on/Off Switch, Whereas Strong Interaction Causes Gradual Change: Folding Transition of a Long Duplex DNA Chain by Poly-L-Lysine. *Biomacromolecules* **2007**, *8* (1), 273−278.
(8) Mann, A.; Richa, R.; Ganguli, M. DNA Condensation by Poly-L-Lysine at the Single Molecule Level: Role of DNA Concentration and Polymer Length. *J. Controlled Release* **2008**, *125* (3), 252−262.
(9) Golan, R.; Pietrasanta, L. I.; Hsieh, W.; Hansma, H. G. DNA Toroids: Stages in Condensation. *Biochemistry* **1999**, *38* (42), 14069−14076.
(10) Zinchenko, A. A.; Yoshikawa, K.; Baigl, D. Compaction of Single-Chain DNA by Histone-Inspired Nanoparticles. *Phys. Rev. Lett.* **2005**, *95* (22), 228101.
(11) Estevez-Torres, A.; Baigl, D. DNA Compaction: Fundamentals and Applications. *Soft Matter* **2011**, *7* (15), 6746−6756.
(12) Post, C. B.; Zimm, B. H. Internal Condensation of a Single DNA Molecule. *Biopolymers* **1979**, *18* (6), 1487−1501.
(13) Grosberg, A. Y.; Erukhimovitch, I. Y.; Shakhnovitch, E. I. On the Theory of Psi-Condensation. *Biopolymers* **1982**, *21* (12), 2413−2432.
(14) Lerman, L. S. A Transition to a Compact Form of DNA in Polymer Solutions. *Proc. Natl. Acad. Sci. U.S.A.* **1971**, *68* (8), 1886−1890.
(15) Zinchenko, A. A.; Yoshikawa, K. Na^+ Shows a Markedly Higher Potential than K^+ in DNA Compaction in a Crowded Environment. *Biophys. J.* **2005**, *88* (6), 4118−4123.
(16) Ellis, R. J.; Minton, A. P. Protein Aggregation in Crowded Environments. *Biol. Chem.* **2006**, *387* (5), 485−497.
(17) Miyoshi, D.; Sugimoto, N. Molecular Crowding Effects on Structure and Stability of DNA. *Biochimie* **2008**, *90* (7), 1040−1051.
(18) Kamata, H.; Zinchenko, A.; Murata, S. Effects of Cationic and Anionic Nanoparticles on the Stability of the Secondary Structure of DNA. *Colloid Polym. Sci.* **2011**, *289* (12), 1329−1335.
(19) Krotova, M. K.; Vasilevskaya, V. V.; Makita, N.; Yoshikawa, K.; Khokhlov, A. R. DNA Compaction in a Crowded Environment with Negatively Charged Proteins. *Phys. Rev. Lett.* **2010**, *105* (12), 128302.
(20) Yoshikawa, K.; Hirota, S.; Makita, N.; Yoshikawa, Y. Compaction of DNA Induced by Like-Charge Protein: Opposite Salt-Effect Against the Polymer-Salt-Induced Condensation with Neutral Polymer. *J. Phys. Chem. Lett.* **2010**, *1* (12), 1763−1766.
(21) Yoshikawa, K.; Matsuzawa, Y. Discrete Phase-Transition of Giant DNA Dynamics of Globule Formation from a Single Molecular Chain. *Physica D* **1995**, *84* (1−2), 220−227.
(22) Gruenwedel, D. W.; Hsu, C. H. Salt Effects on the Denaturation of DNA. *Biopolymers* **1969**, *7* (4), 557−570.
(23) Williams, M. C.; Wenner, J. R.; Rouzina, L.; Bloomfield, V. A. Effect of on on the Overstretching Transition of Double-Stranded DNA: Evidence of Force-Induced DNA Melting. *Biophys. J.* **2001**, *80* (2), 874−881.
(24) Hud, N. V.; Vilfan, I. D. Toroidal DNA Condensates: Unraveling the Fine Structure and the Role of Nucleation in Determining Size. *Annu. Rev. Biophys. Biomol. Struct.* **2005**, *34*, 295−318.
(25) Vilfan, I. D.; Conwell, C. C.; Sarkar, T.; Hud, N. V. Time Study of DNA Condensate Morphology: Implications Regarding the Nucleation, Growth, and Equilibrium Populations of Toroids and Rods. *Biochemistry* **2006**, *45* (26), 8174−8183.
(26) Conwell, C. C.; Vilfan, I. D.; Hud, N. V. Controlling the Size of Nanoscale Toroidal DNA Condensates with Static Curvature and Ionic Strength. *Proc. Natl. Acad. Sci. U.S.A.* **2003**, *100* (16), 9296−9301.
(27) Smith, S. B.; Cui, Y. J.; Bustamante, C. Overstretching B-DNA: The Elastic Response of Individual Double-Stranded and Single-Stranded DNA Molecules. *Science* **1996**, *271* (5250), 795−799.
(28) Bowen, W. R.; Hilal, N.; Lovitt, R. W.; Wright, C. J. Direct Measurement of Interactions Between Adsorbed Protein Layers Using an Atomic Force Microscope. *J. Colloid Interface Sci.* **1998**, *197* (2), 348−352.